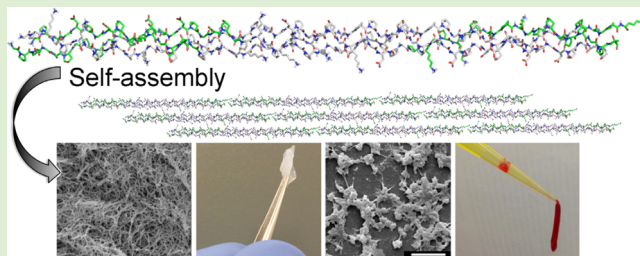


A Nanostructured Synthetic Collagen Mimic for Hemostasis

Vivek A. Kumar, Nichole L. Taylor, Abhishek A. Jalan, Lyahn K. Hwang, Benjamin K. Wang, and Jeffrey D. Hartgerink*

Department of Chemistry, Department of Bioengineering, Rice University, Houston, Texas 77030, United States

ABSTRACT: Collagen is a major component of the extracellular matrix and plays a wide variety of important roles in blood clotting, healing, and tissue remodeling. Natural, animal derived, collagen is used in many clinical applications but concerns exist with respect to its role in inflammation, batch-to-batch variability, and possible disease transfection. Therefore, development of synthetic nanomaterials that can mimic the nanostructure and properties of natural collagen has been a heavily pursued goal in biomaterials. Previously, we reported on the design and multihierachial self-assembly of a 36 amino acid collagen mimetic peptide (KOD) that forms nanofibrous triple helices that entangle to form a hydrogel. In this report, we utilize this nanofiber forming collagen mimetic peptide as a synthetic biomimetic matrix useful in thrombosis. We demonstrate that nanofibrous KOD synthetic collagen matrices adhere platelets, activate them (indicated by soluble P-selectin secretion), and clot plasma and blood similar to animal derived collagen and control surfaces. In addition to the thrombotic potential, THP-1 monocytes incubated with our KOD collagen mimetic showed minimal proinflammatory cytokine (TNF- α or IL-1 β) production. Together, the data presented demonstrates the potential of a novel synthetic collagen mimetic as a hemostat.



Traumatic and surgical bleeding are leading causes of morbidity and mortality worldwide.¹ The dynamic interplay between surgical bleeding and clotting are constant challenges that clinicians face.^{1,2} Pathological clotting resulting in vascular occlusions needs to be avoided while ensuring lack of blood loss.^{3–7} Depending on the method of hemostasis, a variety of instructive cues for tissue regeneration can be presented. For example, mechanical compression of a lesion provides a barrier to bleeding, decreasing perfusion and promoting clotting. Alternatively, heat is a commonly used surgical method for hemostasis and cauterization of microvessels.⁸ While a useful and rapid hemostat, heat-based hemostasis is destructive to tissue architecture, leaves cytotoxic tissue debris, and creates a pro-inflammatory environment.⁹ Hemostatic chemicals such as ethanol, cyanoacrylates, polyvinylalcohol, fibrinogen/fibrin, collagen sponges, or synthetic hydrogels are limited by shelf life, immunogenicity, and cytotoxic byproducts derived from nonhuman or allogenic sources.^{8,10,11}

The use of collagen as a hemostat has been well supported due to its known thrombogenic potential. Collagen-based hemostats offer native tissue scaffolds for blood coagulation and can potentially act as biomimetic nanofibrous templates for instructional tissue regrowth.^{12–22} The impetus for its use is to simulate the native physiologic response to coagulate when collagen in the medial layers of blood vessels are exposed. Coagulation is mediated by collagen-von Willebrand factor (vWF) interaction, collagen platelet/collagen-vWF-platelet interactions, and the physical meshwork of collagen fibrils that entrap blood cells.^{13,23–25} Biologically derived collagen sponges are routinely used as a surgical hemostat, examples of

which include Gelfoam, Avitene, Ultrafoam, and Pahacel. Another commercially available collagen-based hemostat is Vitagel which is a dual factor delivery system using microfibrillar bovine collagen in concert with thrombin and platelet rich plasma (PRP) to cause hemostasis and lay a matrix for wound healing. Current use of Vitagel extends to general, hepatic, cardiac, and orthopedic surgical procedures. While a promising FDA approved technology, a significant drawback stems from the use of bovine collagen which is heterogeneous, xenogenic, and immunogenic.^{26–28}

Alternatively, self-assembling collagen mimetic peptides, short synthetic peptides that replicate portions of the multihierachical self-assembly of natural collagen (Figure 1A) have an interesting potential for biomedical applications,^{29,30} owing to collagen's function in tissue composition and repair.^{31,32} The multihierachal self-assembly of a collagen mimetic peptide from triple helix, to nanofiber, to hydrogel (Figure 1) has been achieved with a recently published peptide (Pro-Lys-Gly)₄(Pro-Hyp-Gly)₄(Asp-Hyp-Gly)₄ from our group (KOD).³³ This triblock peptide is unique since it incorporates collagen's proline-hydroxyproline-glycine repeating unit in the central domain, coupled with the presence of stabilizing interstrand side chain interactions between lysine and aspartate residues.^{34,35} These salt-bridge hydrogen bonds between oppositely charged amino acids serve to stabilize a sticky ended triple helix formation³⁶ that nucleates fiber formation by allowing additional peptide strands to add end-

Received: January 20, 2014

Revised: March 18, 2014

Published: April 2, 2014

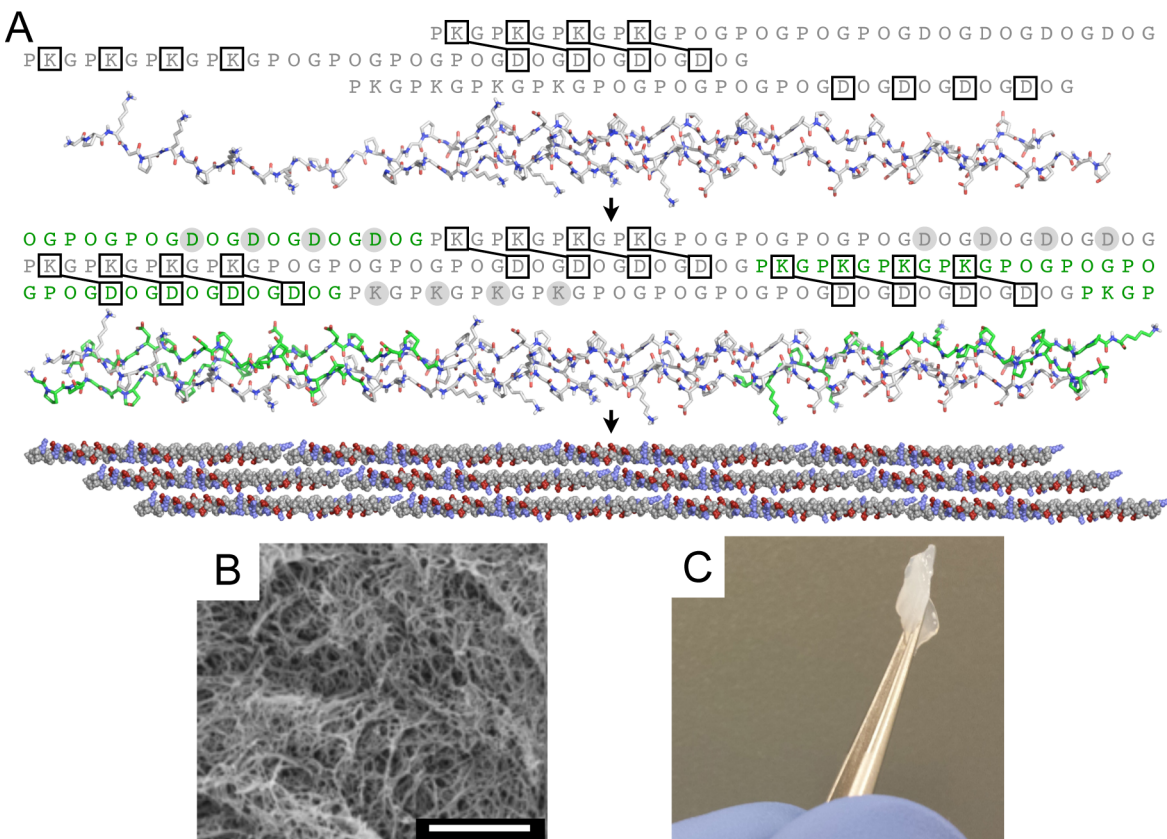


Figure 1. Synthetic collagen mimetic matrices. (A) Hierarchical self-assembly of the KOD peptide into a collagen triple helix with sticky ends indicating Lys-Asp salt bridges and unpaired Lys and Asp residues that allow for supramolecular assembly into fiber networks resembling native collagen, as noted by critical point dried samples under SEM (B), scale bar 1 μ m. (C) Synthetic collagen matrices form a rigid gel that is resistant to mechanical handling by tweezers and other methods.

to-end elongating the triple helix.^{37,38} As a result, self-assembly of KOD nanofibers are observed, which displays the characteristic triple helical packing of natural collagen fibrils.³² In a prior study, we have detailed methods for the design, complete synthesis, purification, and rheological properties of this collagen mimetic protein capable of forming large-scale nanofibrous hydrogels.³⁹

In this study, we demonstrate the novel use of the nanofiber forming collagen mimetic peptide, KOD, for hemostasis. Other peptide hydrogel systems have been proposed for hemostasis. For example, the self-assembling peptide (RADA)₄ (Puramatrix - noted as PURA herein), produced in 1999, has shown the ability to stop bleeding. Alternating hydrophobic and hydrophilic polar residues yield a β -sheet structure that is stabilized by ionic cross-linking at neutral pH and mM salt concentrations.⁴⁰ PURA forms a fibrous meshworks that has been shown to be biocompatible, suitable for tissue engineering, and tested in a variety of applications including hemostasis.^{40–43} While the mechanism behind hemostasis is unknown, it is proposed that the polymer may act as a physical barrier to bleeding without resulting in significant thrombus formation.^{44–46} As a comparison, we have used it as a synthetic hydrogel scaffold control in these studies. Naturally derived rat tail tendon (RTT) acid solubilized collagen was used as a native collagen comparison to KOD; glass, which is known to be have a high propensity for platelet activation, aggregation, and thrombosis, was used as a positive control.^{47,48}

In this report, we show the ability to develop a hemostatic hydrogel composed of designer polypeptide domains that have

three vital hemostatic considerations: (i) noninflammatory physiologically derived substituents, (ii) nanofibrillar morphology to entrap red blood cells and act as a physical barrier to bleeding, and (iii) interaction with platelets. KOD self-assembles into a collagen-like, triple helical, nanofibrous hydrogel that mimics the natural structure of collagen.^{39,49} The hydrogel is shown to cause rapid clotting of whole blood, minimal hemolysis, and significant platelet adhesion and activation, compared to controls. Further, THP-1 monocyte interaction with hydrogel scaffolds do not show upregulation of pro-inflammatory cytokines TNF- α or IL-1 β . Together, these results demonstrate the utility of a novel collagen mimetic peptide hydrogel for hemostasis.

EXPERIMENTAL SECTION

Synthesis and Characterization of Collagen Mimic. Synthetic peptide materials were fabricated using standard Fmoc chemistry for solid-phase peptide synthesis on an Advanced Chemtech Apex 396 multipptide automated synthesizer (Louisville, KY) as detailed.³⁹ The sequence of the peptide is (Pro-Lys-Gly)₄(Pro-Hyp-Gly)₄(Asp-Hyp-Gly)₄ and in single-letter amino acid abbreviations is (P-K-G)₄(P-O-G)₄(D-O-G)₄. For simplicity, the peptide sequence will be referred to as KOD. KOD was synthesized at a scale of 0.15 mM on glycine-preloaded Wang resin. Post synthesis, peptide was cleaved from resin, dissolved and dialyzed against deionized water. Purity was determined using electron spray ionization mass spectroscopy (Bruker MicroTOF, Bruker Daltonics, Billerica, MA). The peptide was subsequently lyophilized and stored at –80 °C until use. For hydrogel samples, the peptide was dissolved in water at a concentration of 2 wt %, annealed at 85 °C, and cooled. Morphology was determined by serial ethanol

dehydration and critical point drying (Electron Microscopy Sciences 850, Hatfield, PA). Samples were sputter coated with 7 nm of gold (Denton Desk V, Moorestown, NJ) and imaged using scanning electron microscopy (FEI Quanta 400 eSEM FEG, Morristown, NJ). We have previously published detailed methods for the design, synthesis, and purification of KOD. The reader is directed to O'Leary et al for further details.³⁹

Control Test Materials. RTT hydrogels (BD Biosciences, San Jose, CA) were polymerized by neutralizing acidified collagen using 1N NaOH, 10X PBS, and DI water, final concentration 4 mg/mL. PURA hydrogels (BD Biosciences) were polymerized by addition of equal volumes of peptide to 1X PBS.⁴⁴ Glass coverslips or tissue culture polystyrene (TCP) were also used as controls where mentioned.

Platelet Adhesion and Morphology. All methods were approved by the Institutional Review Board, Rice University. Static platelet adhesion was determined by incubation of PRP atop KOD, RTT, PURA, glass, or TCP, as described.²² The first 3 mL of blood was discarded. Blood from healthy volunteers was drawn into citrated tubes (Citrated Tubes, BD Biosciences) by venipuncture. Complete blood count was used to determine platelet concentration. PRP was separated by centrifuging citrated whole blood at 200 g for 15 min. PRP fraction was isolated with care not to disturb red blood cell layer. PRP was added to different material surfaces: TCP, glass, RTT gel, KOD gel, and PURA gel for 30 min at 37 °C in a humidified incubator ($n = 6$). After 30 min, PRP was aspirated and surfaces were washed three times with PBS. The number of adherent platelets was quantified using a lactate dehydrogenase cytotoxicity kit (LDH, Roche Diagnostics, Indianapolis, IN). Briefly, 2% Triton X (Sigma, St. Louis, MO) was added to each sample to lyse cells and break down gels. After 30 min, mixtures were centrifuged to remove cellular/material debris and colorimetric LDH quantification substrate was added for 30 min at room temperature. Colorimetric absorbance of 450 nm light was measured and compared to a standard curve of known platelet dilutions. Platelet morphology was determined in a similar way as described above. After incubation of PRP with material surfaces for 30 min, surfaces were washed and fixed with 2.5% glutaraldehyde for 2.5 h. Samples were then serially dehydrated in ethanol and air-dried. Samples were sputter coated with 7 nm of gold and imaged using SEM.

Platelet Activation. To assess platelet activation after adhesion onto scaffolds, soluble P-selectin (sP-selectin) was assayed using ELISA. Two hundred microliters of KOD, RTT, and PURA gels were cast in wells of a 48 well plate resulting in a gel thickness of approximately 2.5 mm. Two hundred microliters of whole blood was incubated atop KOD, RTT, PURA, glass, or TCP for 1 h at 37 °C under static conditions ($n = 5$ for each sample type). Subsequently, the blood was transferred to another tube and EDTA was added to blood to a final concentration of 10 mM. Samples were then centrifuged at 2000g for 10 min to pellet cells and obtain platelet poor plasma (PPP). sP-selectin was detected using ELISA (R&D Systems, Minneapolis, MN).

Plasma Clotting Kinetics. Determination of plasma recalcification profile was done by incubating PPP on surfaces, as previously described.^{47,48} Briefly, blood was drawn, as described above, into ACD tubes, and centrifuged at 2000g for 10 min to obtain PPP. Hydrogel samples (KOD, RTT, PURA) were cast in a 96 well plate, ensuring total well bottom coverage ($n = 6$). One hundred microliters of PPP was added to each sample, and then 100 μ L of 0.025 M CaCl₂ was added to each well to initiate clotting. The plate was then read on a plate reader in 30 s intervals for 50 min at 405 nm at 37 °C to chronicle the clotting response. TCP acted as the positive control, and TCP without the addition of CaCl₂ acted as the negative control. The slope of the linear region of the clotting curve and half-max time was determined.

Whole Blood Clotting Kinetics. The whole blood clotting potential of KOD was determined using static whole blood clotting times compared to control materials: KOD, RTT, PURA, glass, or TCP. As detailed above, blood was drawn via venipuncture into citrated tubes with the first 3 mL being discarded due to potential

contamination with thromboplastin. Hydrogel samples were cast in 24 well plates to cover the bottom of the well (~200 μ L), ($n = 6$) per time point. Clotting of citrated blood was initiated by adding 500 μ L of 0.1 M CaCl₂ to 5 mL of whole blood. One hundred microliters of activated blood was immediately added to surfaces. At each time point 5, 20, 35, and 50 min, 3 mL of distilled water was added for 5 min to each well to lyse red blood cells (RBC) not trapped within the clot. Two hundred microliters of diluted hemoglobin released from lysed RBC was added to a 96 well plate in triplicate for each sample and time point and read for absorbance at 540 nm. Because the absorbance is indicative of RBC not trapped within the clot, it is inversely related to clot size.

Hemolytic Potential of Materials. Rupture of RBC due to interaction with material surfaces was determined by incubating materials with diluted blood.⁵⁰ Briefly, blood drawn into ACD tubes were diluted 50X in 0.9% saline. One hundred microliters of diluted blood was incubated with 100 μ L samples of KOD, RTT, PURA, or empty microcentrifuge tube (negative control) for 2 h at 37 °C with mild agitation ($n = 6$). Blood diluted in DI water in a microcentrifuge tube was used as the positive control. Post incubation, the supernatant was retrieved, centrifuged (1000g, 10 min) to remove RBC/debris, and 100 μ L aliquots transferred into a 96 well plate read at 545 nm. Percent hemolysis was determined as a function of $[(\text{Abs}_{\text{Sample}} - \text{Abs}_{\text{Negative Control}})/\text{Abs}_{\text{Positive Control}}]^{50}$.

Proinflammatory Potential of Materials. Assessment of proinflammatory cytokine secretion from THP-1 cells' interaction with KOD, RTT, PURA, glass, or TCP was assessed as previously published.⁴⁷ One hundred microliters gels were cast in quadruplicate in 48 well plates ($n = 6$). Macrophages differentiated to M1 (20 ng/mL IFN- γ +LPS) and M2 (20 ng/mL IL-4) phenotype were used as cell controls. THP-1 cells in suspension were suspended in media and incubated at a concentration of 1 M cells/well atop scaffolds. Media aliquots were assayed for inflammatory cytokines (IL-1 β , TNF- α) at 24 h using ELISA (Biologend, CA).

Statistical Analysis. Data is represented as mean \pm standard deviation. Differences between paired data were compared using Student's t-test, and ANOVA with Tukey post hoc analysis for multiple comparisons of parametric data and Kruskal-Wallis ANOVA with Dunn's post hoc analysis for nonparametric data. Values of ($p < 0.05$) were considered statistically significant.

RESULTS AND DISCUSSION

Rationale Design of Nanostructured Collagen Mimics. KOD, (Pro-Lys-Gly)₄(Pro-Hyp-Gly)₄(Asp-Hyp-Gly)₄, peptides were prepared using solid phase peptide synthesis and were purified using dialysis and lyophilization as described previously.³⁹ Peptides were dissolved in water at 2 wt %, warmed to 85 °C, and then cooled, allowing annealing of individual peptides into triple helices and subsequent assembly into a nanofibrous hydrogel, (Figure 1A). The structure of KOD showed the ability to form extracellular matrix (ECM) mimetic structures at the chemical, triple helical, and nanofiber scales (Figure 1B), yielding large-scale "handle-able" hydrogels (Figure 1C). Further, the KOD peptide sequence has design elements that are known to be intrinsically pro-hemostatic, such as the contiguous POG amino acid triplet sequence (Figure 1). Together, these design elements suggest the potential for prohemostatic properties, similar to native collagen.

Use of Collagen Mimetic Scaffolds for Hemostasis. Utility of collagen mimics for hemostasis has yet to be described. KOD presents theoretical analogues to native collagen in protein structure and folding, as well as procoagulatory moieties that may promote platelet adhesion and activation. To test the hemostatic properties of KOD, we first assessed its inflammatory potential. THP-1 monocytic leukemia cells were seeded on scaffolds. Cells did not show significantly different proinflammatory (TNF- α and IL-1 β)

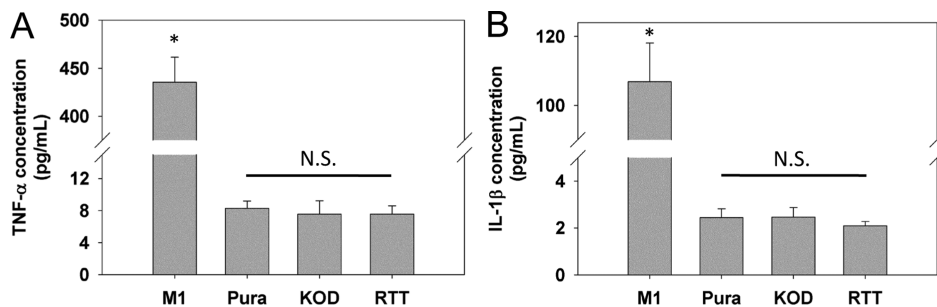


Figure 2. Inflammatory potential of materials. Proinflammatory markers (A) TNF- α and (B) IL-1 β for synthetic materials. Concentrations of cytokines on scaffolds PURA, KOD, and RTT were all significantly lower than LPS stimulated M1 macrophages, $n = 6$, * $p < 0.01$.

Table 1. Comparative Hemostatic Properties of Engineered Collagen Matrices

material	platelet adhesion (platelets/mm ²) $\times 10^3$	sP-selectin concentration (ng/mL)	plasma recalcification time (min)	inflammatory cytokine TNF- α (pg/mL)	inflammatory cytokine IL-1 β (pg/mL)
KOD	2.62 \pm 0.35 $^\beta$	35.3 \pm 2.7 $^\beta$	13.1 \pm 1.1 $^\alpha$	7.52 \pm 1.6 $^\delta$	2.46 \pm 0.40 $^\delta$
RTT	2.15 \pm 0.33 $^\beta$	28.5 \pm 0.8 $^\alpha$	13.6 \pm 1.4 $^\alpha$	7.54 \pm 1.04 $^\delta$	2.09 \pm 0.17 $^\delta$
glass	2.15 \pm 0.13 $^\beta$	29.4 \pm 1.3 $^\alpha$	NA	NA	NA
TCP	1.35 \pm 0.11 $^\alpha$	27.6 \pm 1.8 $^\alpha$	11.4 \pm 0.2 $^\alpha$	435 \pm 25.8 $^{\alpha,\epsilon}$	106 \pm 11.2 $^{\alpha,\epsilon}$
PURA	1.03 \pm 0.02 $^\gamma$	23.2 \pm 1.4 $^\gamma$	14.2 \pm 0.5 $^\alpha$	8.26 \pm 0.92 $^\delta$	2.43 \pm 0.38 $^\delta$

^aLPS activated THP-1 monocytes on TCP positive control tested for inflammatory cytokines. Kruskal–Wallis ANOVA: $p < 0.05$ between different Greek symbols (α,β,γ), $p < 0.01$ between different Greek symbols (δ,ϵ).

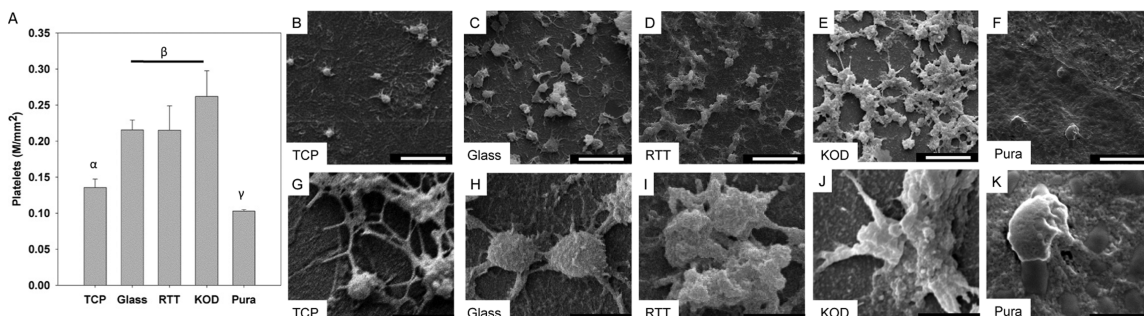


Figure 3. Platelet adhesion to test surfaces. (A) KOD surfaces displayed similar levels of platelet adhesion to glass and RTT, significantly higher than TCP. Low-magnification images of platelets adhered to surfaces qualitatively showed platelet density: (B) TCP, (C) glass, (D) RTT, (E) KOD, (F) PURA. Scale bar: 10 μm . At high magnification, platelet spreading and clumping was indicative of higher platelet activation: (G) TCP, (H) glass, (I) RTT, (J) KOD, (K) PURA. Scale bar: 2 μm . Noncritical point dried (air-dried) samples did not show nanofibrous structure of underlying matrix. ($n = 6$, $p < 0.05$ between different Greek symbols).

marker expression when seeded on different scaffolds compared to positive control ($p < 0.01$, $n = 6$, Figure 2, Table 1). Data was compared to LPS activated cells, which showed significantly greater cytokine expression ($p < 0.01$). Together, this indicates that KOD does not promote a proinflammatory response.

Platelet adhesion and morphology is indicative of the clotting potential of materials. PRP incubated atop hydrogel scaffolds showed higher adhesion to KOD, than RTT or glass, used as positive control ($p < 0.05$). Platelet adhesion onto collagen mimetic scaffolds was significantly higher than negative control, TCP, and PURA ($p < 0.05$, $n = 6$, Figure 3A, Table 1). Platelets were spread with observable filopodial extensions on TCP, glass, RTT and KOD (Figure 3B–E,G–J). PURA had fewer adherent platelets with a more rounded morphology (Figure 3F,K). Further, KOD (Figure 3E,J) and RTT (Figure 3D,I) surfaces showed greater clumping and aggregation of platelets ($n = 6$). Note that samples were fixed in glutaraldehyde, dehydrated, and air-dried (not critical point dried). Thus, due to processing conditions nanofibrous morphology of matrices is

not noted in Figure 3. In addition to total number of platelets and qualitative observation of platelet morphology, we substantiated platelet activation by quantifying soluble P-selectin (sP-selectin). sP-selectin released from platelets was measured using ELISA (Figure 4). sP-selectin concentration due to interaction of platelets with KOD was significantly higher than all other tested materials, ($p < 0.01$). Glass, TCP, and RTT showed similar sP-selectin concentrations ($p > 0.1$). All samples showed significantly higher sP-selectin secretion than PURA ($p < 0.05$, $n = 5$, Table 1). Differences in platelet adhesion may have been due to nonspecific plasma protein adsorption onto different surfaces (TCP, glass, RTT, and KOD) and subsequent platelet adhesion, and entrapment of platelets in nanofibrous matrices.

With respect to platelet-collagen interaction, the formation of the thrombus proceeds in two key steps; adhesion of the platelets to the collagen followed by collagen-mediated platelet activation. Initial adhesion of the platelets to collagen is mediated by the platelet receptor GPIb that binds to the A3 domain of the plasma glycoprotein vWF that in turn binds to

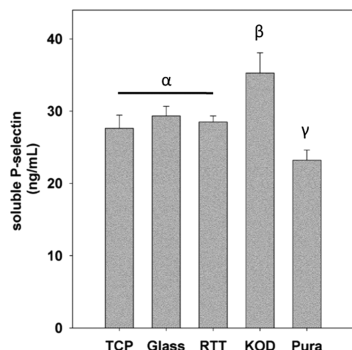


Figure 4. Soluble P-selectin from platelet interaction with KOD. sP-selectin concentration detected by ELISA ($n = 5$, $p < 0.05$ between different Greek symbols).

collagen⁵¹ and activating integrin-based receptors.^{52,53} Further, GPVI, an Ig-like glycoprotein, is a key platelet receptor that plays a crucial role in platelet activation.⁵⁴ It has been shown that GPVI undergoes constitutive dimerization and binds to a variety of peptides containing contiguous POG triplet repeats and initiates a signaling cascade responsible for much of the downstream thrombus formation.^{51,55–57} In our system (POG)_n repeats may be presented in the context of an unfolded, soluble peptide, a folded triple helix as well as

assembled nanofibrous triple helices that may initiate platelet adhesion and activation. Overall, the fibrillar morphology of the KOD and the putative triple helical arrangement within fiber place multiple POG tandem repeats on the fiber surface that are conducive to GPVI binding.^{51,55–57}

To further understand the interaction of blood with KOD and its hemostatic potential, we studied two other blood components' interaction with KOD: blood plasma and whole blood. We quantified plasma clotting potential by incubating scaffolds with platelet poor plasma, PPP. PPP without Ca^{2+} addition did not show a significant increase in turbidity and did not show plasma clotting over the 50 min test period. With the addition of Ca^{2+} , TCP showed initiation of plasma clotting after about 6 min (Figure 5A). Hydrogel scaffolds KOD and PURA showed similar kinetic profiles (Figure 5B), indicating similar plasma clotting potential. Further, KOD and RTT showed slightly lower half-max time compared to PURA ($p > 0.05$) which were higher than TCP ($p < 0.05$, $n = 6$, Table 1).

We quantified whole blood clotting potential by incubating scaffolds with recalcified whole blood. Clots that formed on material surfaces trapped RBC within fibrin matrices. Free RBC, outside of the clot, were lysed when DI water was added in excess. As such, absorbance values early in the assay indicate more hemoglobin presence and decrease with larger clot formation. KOD showed a significantly faster whole blood clotting rate at the 20 min time point compared to RTT,

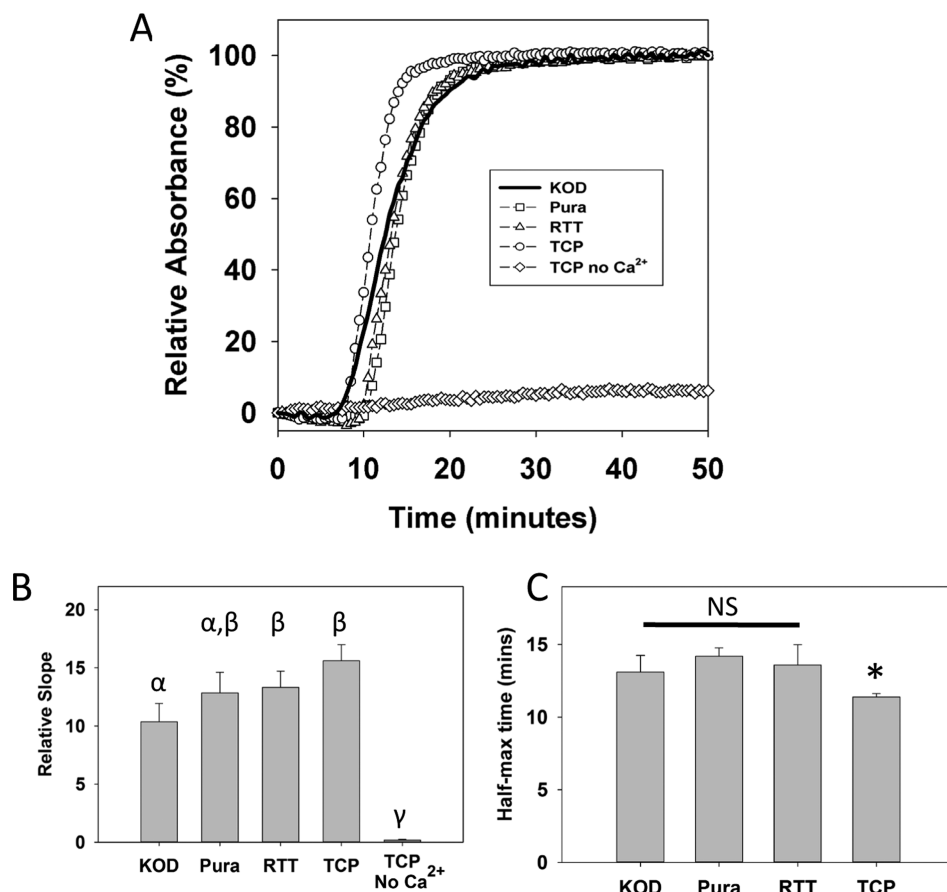


Figure 5. Plasma recalcification profile on surfaces. (A) PPP + Ca^{2+} incubated on KOD, RTT, PURA, and TCP surfaces showed characteristic clotting kinetics as a function of time, compared to negative control PPP without Ca^{2+} on TCP. Data was normalized to respective sample absorbance at 50 min. Negative control absorbance was normalized to TCP 50 min absorbance. (B) PPP clotting rate as measured by the slope of linear region of the curves showed no significant difference for the surfaces. (C) Clotting time as determined by half-max time showed that hydrogel surfaces clotted more quickly than TCP. ($n = 6$, $*p < 0.05$ between different Greek symbols).

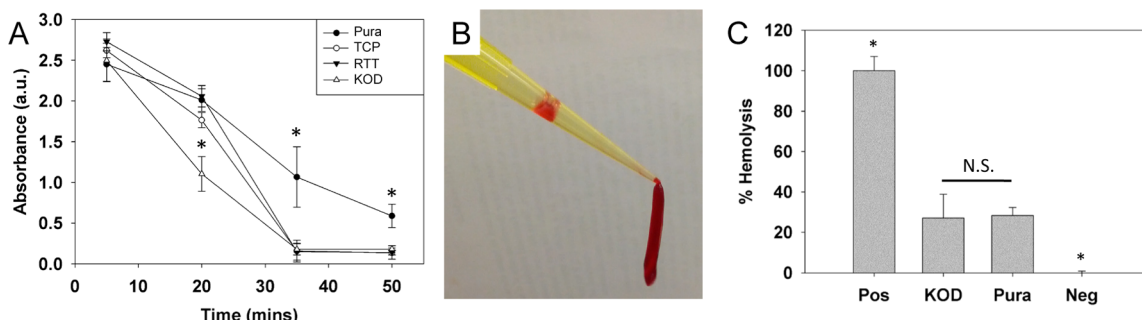


Figure 6. Whole blood clotting on material surfaces. (A) Rate of whole blood clotting was inversely related to absorbance. PURA showed slowest clotting times with significantly higher absorbance at 35 and 50 min, * $p < 0.01$. KOD shows faster initiation of clotting with a significantly lower absorbance at 20 min, * $p < 0.01$. Whole blood clotting times were quantified on materials surfaces. (B) A large blood clot formed atop KOD was aspirated into a 200 μL pipet tip. (C) Hemolysis due to interaction with KOD or PURA quantified and compared to positive (DI water) control or negative (isotonic solution) control, * $p < 0.01$.

PURA, or TCP ($p < 0.05$). PURA did not clot blood to the same extent as KOD, RTT, or TCP at later 35 and 50 min time points ($p < 0.05$) (Figure 6A, $n = 6$). Figure 6B shows a clot on the end of a 200 μL pipet tip that has formed on top of the KOD hydrogel scaffold. Incubation of blood with materials allowed for quantification of potential hemolysis. Synthetic collagen KOD showed similarly low hemolytic potential to PURA (Figure 6 C, $n = 6$). Both KOD ($27.1 \pm 11.0\%$) and PURA ($28.3 \pm 4.0\%$) showed greater hemolysis than negative control ($p < 0.01$).

The distinct nanofibrillar morphology of KOD is similar to native nanostructured collagen and fibrin that are pivotal in abrogating physiologic bleeding and mediating wound healing. With respect to hemostasis, fibrin clots generate a meshwork that entrap red blood cells (RBC), provide a hemostatic plug, and act as the scaffold for tissue regeneration. Similarly, exposed tissue collagen acts in a manner to activate formation of platelet clots and as a barrier hemostat, to prevent hemorrhaging. As such, we sought to analyze specific interactions of blood components responsible for hemostasis with KOD. Native fibrin and collagen act as template matrices for tissue regeneration after plasmin mediated fibrinolysis/macrophage mediated clearing of debris in native tissue. Similarly, synthetic collagen mimics such as KOD may provide an opportunity to augment wound healing. Of note is Vitagel, a commercially available hemostat that combines the patient's PRP, bovine collagen, and thrombin to create a fibrin/collagen/platelet clot. Clinical trials have demonstrated the use of Vitagel as a hemostat that allows for improved tissue regeneration. While a promising strategy, xenogenic collagen presents concerns associated with immunogenicity of bovine collagen and thrombin, potential allergic reaction, viral/prion transmission, and potential batch-to-batch variability.^{27,28} KOD may be a viable alternative for the use of native collagen in this and other applications. Repeatable and reliable solid phase peptide synthesis, quality control with mass spectroscopy, HPLC, and other analytical methods ensures purity and homogeneity. While this study investigated the use of KOD without mixtures of thrombin or PRP, future studies could involve additional factors to aid in clotting or wound regeneration.

CONCLUSION

We have demonstrated the use of important chemistries that have aided in the engineering of triple helices that form stable 3D nanofibrous hydrogels in a novel collagen mimetic peptide.³⁹ We have shown the utility of these matrices as a

viable hemostat based on key features of the material, chemical, and nanostructure. First, KOD is composed of noninflammatory materials with low TNF- α / IL-1 β levels. Second, the engineered synthetic collagen forms long-range nanofibers that may promote adhesion and activation of platelets and clotting plasma. Third, KOD matrices have specific moieties that may interact with platelets activating them. The aforementioned factors suggest a possible mechanism for hemostasis on KOD surfaces. As a next step, we envision expanding the repertoire of the nanostructured KOD synthetic collagen family to include moieties that may promote wound healing and other key aspects of native tissue. Additionally, we plan to study KOD in surgical bleeding in higher animal models. In addition to extravascular hemostasis, use of KOD can be extended to a variety of intravascular pathologies such as filling of graft-vessel wall space, saccular aneurysms, and therapeutic chemoembolization.⁵⁸

AUTHOR INFORMATION

Corresponding Author

E-mail: jdh@rice.edu. Tel: (713) 348-4142.

Author Contributions

The manuscript was written through contributions of all authors. All authors have given approval to the final version of the manuscript.

Notes

The authors declare no competing financial interest.

ACKNOWLEDGMENTS

The authors would like to thank Angie B. Woodley for her assistance in blood draws and Professor Miguel A. Cruz for his useful insight. The work presented in this manuscript was supported by grants from the NIH (R01 DE021798), NSF (DMR-1206899), and the Robert A. Welch Foundation (Grant C1557). V.A.K. gratefully acknowledges his support through an NIH F32 award (F32 DE023696).

REFERENCES

- (1) Samudrala, S. *AORN J.* **2008**, *88*, S2–S11.
- (2) Sileski, B.; Achneck, H. E.; Lawson, J. H. *Vascular* **2008**, *16* (Suppl 1), S22–S28.
- (3) Naitoh, Y.; Kawauchi, A.; Kamoi, K.; Soh, J.; Okihara, K.; Hyon, S. H.; Miki, T. *Urology* **2013**, *81*, 1095–1100.
- (4) Shoffstall, A. J.; Atkins, K. T.; Groynom, R. E.; Varley, M. E.; Everhart, L. M.; Lashof-Sullivan, M. M.; Martyn-Dow, B.; Butler, R. S.; Ustin, J. S.; Lavik, E. B. *Biomacromolecules* **2012**, *13*, 3850–3857.

- (5) Saif, R.; Jacob, M.; Robinson, S.; Amer, A.; Kei-Hui, D.; Sen, G.; Manas, D.; White, S. *Surg. Laparosc. Endosc. Percutan. Tech.* **2011**, *21*, 131–141.
- (6) Smeets, R.; Gerhards, F.; Stein, J. M.; Paz, R. M.; Vogt, S.; Pautke, C.; Weitz, J.; Kolk, A. *J. Biomed. Mater. Res., Part A* **2011**, *96*, 177–185.
- (7) Bertram, J. P.; Williams, C. A.; Robinson, R.; Segal, S. S.; Flynn, N. T.; Lavik, E. B. *Sci. Transl. Med.* **2009**, *1*, 11ra22.
- (8) Boucher, B. A.; Traub, O. Achieving hemostasis in the surgical field. *Pharmacotherapy* **2009**, *29*, 2S–7S.
- (9) Lantis, J. C., II; Durville, F. M.; Connolly, R.; Schwartzberg, S. D. *J. Laparoendosc. Adv. Surg. Tech. A* **1998**, *8*, 381–394.
- (10) Sileshi, B.; Achneck, H.; Ma, L.; Lawson, J. H. *Vascular* **2010**, *18*, 197–204.
- (11) Cheng, C. M.; Meyer-Massetti, C.; Kayser, S. R. *Clin. Ther.* **2009**, *31*, 32–41.
- (12) Stoppato, M.; Carletti, E.; Maniglio, D.; Migliaresi, C.; Motta, A. *J. Tissue Eng. Regener. Med.* **2013**, *7*, 161–168.
- (13) Cejas, M. A.; Kinney, W. A.; Chen, C.; Vinter, J. G.; Almond, H. R., Jr.; Balss, K. M.; Maryanoff, C. A.; Schmidt, U.; Breslav, M.; Mahan, A.; Lacy, E.; Maryanoff, B. E. *Proc. Natl. Acad. Sci. U.S.A.* **2008**, *105*, 8513–8518.
- (14) Pugh, N.; Simpson, A. M.; Smethurst, P. A.; de Groot, P. G.; Raynal, N.; Farndale, R. W. *Blood* **2010**, *115*, 5069–5079.
- (15) Farndale, R. W.; Siljander, P. R.; Onley, D. J.; Sundaresan, P.; Knight, C. G.; Barnes, M. J. *Biochem. Soc. Symp.* **2003**, 81–94.
- (16) Chattopadhyay, S.; Murphy, C. J.; McAnulty, J. F.; Raines, R. T. *Org. Biomol. Chem.* **2012**, *10*, 5892–5897.
- (17) Kotch, F. W.; Raines, R. T. *Proc. Natl. Acad. Sci. U.S.A.* **2006**, *103*, 3028–3033.
- (18) Kar, K.; Ibrar, S.; Nanda, V.; Getz, T. M.; Kunapuli, S. P.; Brodsky, B. *Biochemistry* **2009**, *48*, 7959–7968.
- (19) Kar, K.; Amin, P.; Bryan, M. A.; Persikov, A. V.; Mohs, A.; Wang, Y. H.; Brodsky, B. *J. Biol. Chem.* **2006**, *281*, 33283–33290.
- (20) Kumar, V. A.; Martinez, A. W.; Caves, J. M.; Naik, N.; Haller, C. A.; Chaikof, E. L. *Biomed. Mater.* **2014**, *9*, 011002.
- (21) Kumar, V. A.; Caves, J. M.; Haller, C. A.; Dai, E.; Li, L.; Grainger, S.; Chaikof, E. L. *Biomater. Sci.* **2013**, *1*, 11.
- (22) Kumar, V. A.; Caves, J. M.; Haller, C. A.; Dai, E.; Liu, L.; Grainger, S.; Chaikof, E. L. *Acta Biomater.* **2013**, *9*, 8067–8074.
- (23) Hatsuoka, M.; Seiki, M.; Sasaki, K.; Kashii, A. *Thromb. Res.* **1986**, *42*, 407–412.
- (24) Abbott, W. M.; Austen, W. G. *Surgery* **1975**, *78*, 723–729.
- (25) Cejas, M. A.; Chen, C.; Kinney, W. A.; Maryanoff, B. E. *Bioconjugate Chem.* **2007**, *18*, 1025–1027.
- (26) Meade, K. R.; Silver, F. H. *Biomaterials* **1990**, *11*, 176–180.
- (27) Takayama, E.; Ikeda, M.; Tsuru, S.; Ogura, M.; Kitahara, S.; Inouye, T.; Healy, G. B. *J. Laryngol. Otol.* **1992**, *106*, 704–708.
- (28) Lynn, A. K.; Yannas, I. V.; Bonfield, W. *J. Biomed. Mater. Res., Part B* **2004**, *71*, 343–354.
- (29) Kotch, F. W.; Raines, R. T. *Proc. Natl. Acad. Sci. U.S.A.* **2006**, *103*, 3028–3033.
- (30) Ottani, V.; Martini, D.; Franchi, M.; Ruggeri, A.; Raspanti, M. *Micron* **2002**, *33*, 587–596.
- (31) Ottani, V.; Raspanti, M.; Ruggeri, A. *Micron* **2001**, *32*, 251–260.
- (32) Ramachandran, G. N.; Kartha, G. *Nature* **1955**, *176*, 593–595.
- (33) O’Leary, L. E. R.; Fallas, J. A.; Bakota, E. L.; Kang, M. K.; Hartgerink, J. D. *Nat. Chem.* **2011**, *3*, 821–828.
- (34) Rele, S.; Song, Y. H.; Apkarian, R. P.; Qu, Z.; Conticello, V. P.; Chaikof, E. L. *J. Am. Chem. Soc.* **2007**, *129*, 14780–14787.
- (35) Fallas, J. A.; Gauba, V.; Hartgerink, J. D. *J. Biol. Chem.* **2009**, *284*, 26851–26859.
- (36) Bella, J.; Eaton, M.; Brodsky, B.; Berman, H. M. *Science* **1994**, *266*, 75–81.
- (37) Pandya, M. J.; Spooner, G. M.; Sunde, M.; Thorpe, J. R.; Rodger, A.; Woolfson, D. N. *Biochemistry* **2000**, *39*, 8728–8734.
- (38) Woolfson, D. N. *Biopolymers* **2010**, *94*, 118–127.
- (39) O’Leary, L. E.; Fallas, J. A.; Bakota, E. L.; Kang, M. K.; Hartgerink, J. D. *Nature Chem.* **2011**, *3*, 821–828.
- (40) Luo, Z.; Zhang, S. *Chem. Soc. Rev.* **2012**, *41*, 4736–4754.
- (41) Luo, Z.; Yue, Y.; Zhang, Y.; Yuan, X.; Gong, J.; Wang, L.; He, B.; Liu, Z.; Sun, Y.; Liu, J.; Hu, M.; Zheng, J. *Biomaterials* **2013**, *34*, 4902–4913.
- (42) Zou, Z.; Zheng, Q.; Wu, Y.; Guo, X.; Yang, S.; Li, J.; Pan, H. *J. Biomed. Mater. Res., Part A* **2010**, *95*, 1125–1131.
- (43) Nune, M.; Kumaraswamy, P.; Krishnan, U. M.; Sethuraman, S. *Curr. Protein Pept. Sci.* **2013**, *14*, 70–84.
- (44) Ellis-Behnke, R. G.; Liang, Y. X.; Tay, D. K.; Kau, P. W.; Schneider, G. E.; Zhang, S.; Wu, W.; So, K. F. *Nanomed.: Nanotechnol. Biol. Med.* **2006**, *2*, 207–215.
- (45) Hartgerink, J. D. *Nat. Nanotechnol.* **2006**, *1*, 166–167.
- (46) Ellis-Behnke, R. *Nanomed. Nanobiotechnol.* **2011**, *3*, 70–78.
- (47) Motlagh, D.; Yang, J.; Lui, K. Y.; Webb, A. R.; Ameer, G. A. *Biomaterials* **2006**, *27*, 4315–4324.
- (48) Motlagh, D.; Allen, J.; Hoshi, R.; Yang, J.; Lui, K.; Ameer, G. J. *Biomed. Mater. Res., Part A* **2007**, *82*, 907–916.
- (49) Fallas, J. A.; O’Leary, L. E.; Hartgerink, J. D. *Chem. Soc. Rev.* **2010**, *39*, 3510–3527.
- (50) Dey, J.; Xu, H.; Nguyen, K. T.; Yang, J. *J. Biomed. Mater. Res., Part A* **2010**, *95*, 361–370.
- (51) Herr, A. B.; Farndale, R. W. *J. Biol. Chem.* **2009**, *284*, 19781–19785.
- (52) Emsley, J.; Knight, C. G.; Farndale, R. W.; Barnes, M. J.; Liddington, R. C. *Cell* **2000**, *101*, 47–56.
- (53) Saelman, E. U. M.; Nieuwenhuis, H. K.; Hese, K. M.; Degroot, P. G.; Heijnen, H. F. G.; Sage, E. H.; Williams, S.; McKeown, L.; Gralnick, H. R.; Sixma, J. J. *Blood* **1994**, *83*, 1244–1250.
- (54) Kehrel, B.; Wierwille, S.; Clemetson, K. J.; Anders, O.; Steiner, M.; Knight, C. G.; Farndale, R. W.; Okuma, M.; Barnes, M. J. *Blood* **1998**, *91*, 491–499.
- (55) Horii, K.; Kahn, M. L.; Herr, A. B. *Blood* **2006**, *108*, 936–942.
- (56) Jung, S. M.; Moroi, M.; Soejima, K.; Nakagaki, T.; Miura, Y.; Berndt, M. C.; Gardiner, E. E.; Howes, J. M.; Pugh, N.; Bihani, D.; Watson, S. P.; Farndale, R. W. *J. Biol. Chem.* **2012**, *287*, 30000–30013.
- (57) Berlanga, O.; Bori-Sanz, T.; James, J. R.; Frampton, J.; Davis, S. J.; Tomlinson, M. G.; Watson, S. P. *J. Thromb. Haemostasis* **2007**, *5*, 1026–1033.
- (58) Lubarsky, M.; Ray, C.; Funaki, B. *Semin. Interventional Radiol.* **2010**, *27*, 99–104.